Andean growth and monsoon winds drive landscape evolution at SW margin of South America

Aurélie Coudurier-Curveur [1,2], Robin Lacassin [1] and Rolando Armijo [1]

[1] *Institut de Physique du Globe de Paris, Sorbonne Paris Cité, Univ. Paris Diderot, UMR 7154 CNRS, France*

[2] *Earth Observatory of Singapore, Nanyang Technological University, Singapore*

Coudurier@ipgp.fr

Lacassin@ipgp.fr *(corresponding author)*

Armijo@ipgp.fr

Supplementary information

A/ Numerical description of APERO Landscape Model

In this study, we aim to model, at first-order, drainage system development over an uplifting area (larger than 150 km^2) since Late Miocene (< 10 Ma) in relation to a spatially variable precipitation gradient. Many numerical landscape evolution models (LEM) have been developed during the last 20 years to account for different time and space scales investigations, in one or more dimensions. These large time scale physical models mainly use (semi-) empirical laws and can account for several processes such as tectonic uplift, precipitation rates and even surface diffusion. We may cite SIBERIA (Willgoose et al., 1991), CAESAR (Coulthard et al., 2002; Van de Wiel et al., 2007) GOLEM (Tucker and Slingerland, 1994), CASCADE (Braun & Sambridge, 1997; Van Der Beek & Braun, 1999), CHILD (Tucker & Bras, 2000), EROS (Davy and Crave, 2000; Crave & Davy, 2001), and APERO/CIDRE (Carretier & Lucazeau, 2005; Carretier et al., 2009) as the most often used and cited models. They differ from each other with respect to both time and space scales used, to the processes accounting for tectonic uplift, infiltration, evaporation, diffusion type, water distribution, etc. to the way the governing equations are numerically solved. We chose to use the landscape model APERO because it is suitable for modeling interactions between tectonics, climate and erosion over large time and spatial scales, up to several million years and several hundreds of kilometers and accounts also for non-uniform tectonic uplift. Furthermore, this model has already been used for tectonic investigations in Central Chile (Farías, 2007; Quezada, 2008). This makes it easier to calibrate and compare with. However, many parameters in this model cannot be accurately constrained so that the analyses remain semi-quantitative.

APERO code models landscape evolution by routing water and sediments over a grid of regular cells from the highest to the lowest, changing elevations according to sediment production resulting from hillslope erosion, alluvial transport and bedrock incision. We detail step by step here the numerical implementation of the APERO code owing to descriptions from [Carretier, 2000], [Carretier and Lucazeau, 2005] and also from the Apero User's guide (S. Carretier, 2004).

First, water is distributed on the entire grid depending the input precipitation grid and then propagates according to the selected distribution, that ensure conservation of water (Eq.1), between (1) the steepest descent mode (water from a cell is directly distributed to the lowest neighbouring cell) and (2) the multiple flow process (water from a cell is distributed to all the neighbouring cells according to their respective slope). This process results in the characterization of the water discharge Q_{fOUT} for each cell over the grid. Rainfall is supposed to represent the effective discharge due to cumulative rainfall events over a given time scale.

Then, the model is considering a cell i, which is either a pure bedrock cell or a bedrock cell covered with sediments. If that cell is not covered with sediments, the model computes the **sediment output due to bedrock diffusion processes**, $Q_{snldiff}$ ([L^3T^{-1}]) (Eq.S1), or diffusive transport flux, given by a non-linear diffusion equation (Roering et al., 1999) (Eq.S2) :

$$Q_{snldiff} = \nabla . q_{snldiff} \qquad \text{(Eq.S1)}$$

where $$q_{snldiff} = -\kappa \frac{\nabla h_s}{1-(\frac{\nabla h_s}{Sc})^2}$$ (Eq.S2)

With h_s, the ground elevation integrated over the cell size, Sc the critical slope corresponding to the material gradient of repose (in that case, $Sc = Sc_{br}$ for material gradient of repose for bedrock) and κ a diffusion coefficient ([L^2T^{-1}]) ($\kappa = \kappa_{br}$ for bedrock diffusion coefficient). Other LEM (eg. GOLEM (Tucker and Slingerland, 1994)) do not take into account this non-linear process. In our case study, the formation of deep and straight channels enhances landslides processes justifying the use of APERO to consider that process.

However, if the cell i is covered with sediments, the model computes the **sediment output due to sediment diffusion processes** using (Eq.S1 and Eq.S2) with $Sc = Sc_{sed}$ for material gradient of repose for sediments and $\kappa = \kappa_{sed}$ for sediment diffusion coefficient.

Then, this possible sediment output due to sediment diffusion is compared to the available stock of sediments on the cell i: (1) if the sediment output is lower than the stock, the final sediment output corresponds to the difference between both values; (2) if the sediment output is greater than the stock, then the stock of sediments becomes null and the model computes a new sediment output due to diffusion processes for bedrock using (Eq.S1 and Eq.S2) with $Sc = Sc_{br}$ and $\kappa = \kappa_{br}$.

These respective resulting sediment outputs correspond to **available sediments for alluvial transport**.

Later, the model computes the alluvial transport capacity (Eq.S3), which corresponds to the **maximum possible transport of sediments by water processes**. It is expressed, for both large time and space scales, as Q_{sal} ([L^3T^{-1}]) and depends on the total water discharged Q_{fOUT} ([L^3T^{-1}]), the local topographic slope S_{ij} and the alluvial transport coefficient K_{al} following the equation:

$$Q_{sal} = K_{al} {Q_{fOUT}}^{\alpha} {S_{ij}}^{\beta}$$ (Eq.S3)

where K_{al} ([$L^{3-3\alpha} T^{\alpha-1}$]) is a positive coefficient, α and β are two exponents that determine the degree of non linearity of the transport law. See Section C.2 for details about the assigned values of α, β and K_{al}.

A new balance is calculated between the maximum transport capacity Q_{sal} and the sediment output due to diffusion processes $Q_{snldiff}$. If the balance is negative, that is to say, the transport capacity is lower than the available sediments for transport, then alluvial transport of sediments is rated by the maximum transport capacity. If the balance is positive, all the available sediments will be transported and the model will compute the **sediment output due to bedrock incision** Qbr following a stream power law:

$$Q_{br} = K_{br} {Q_{fOUT}}^{m} {S_{ij}}^{n}$$ (Eq.S4)

with K_{br} ($[L^{1-3m}\ T^{m-1}]$) the bedrock erosion coefficient. m and n are two exponents whose values, comprised between 0 and 2, are still debated (see Section C.2). K_{br} ($[L^3T^{-1}]$) is not clearly determined in the literature (see Section C.2). It scales with lithology and precipitation rates. However, there is no direct natural constraint for this parameter that makes it difficult to characterize and interpret compared to real case studies. Furthermore, resulting sediments from the bedrock incision process cannot exceed the residual alluvial transport capacity.

Then, a balance of the different fluxes (deposition, diffusion, transport, erosion) occurring on the cell I is done, later used to calculate the elevation change on the cell I in agreement with the conservation law of mass for sediments.

B/ Initial and boundary conditions

The boundary conditions for our numerical experiments are described in more detail here and shown graphically on Figure S1. These boundary conditions are the same for all the experiments presented here.

B.1 Uplift rates

From geological and geomorphic observations (see discussion in Part 2 of the paper), we make the hypothesis that the whole coastal topography has been deeply incised in response to tectonic uplift, so we use published incision rates estimates to constrain the two different uplift rates at each side of the margin.

At the western side, coastal incision rates estimates correspond to the ratio between the height of incision and the onset of incision. Height of incision is determined by the knickpoint height (1000 m) that also corresponds to the difference amplitude between the Atacama Pediplain base-level and the ocean base-level (see Fig. 4 & 5 and Fig. S1-A). Onset time of incision in North Chile is constrained by the age of the latest surface deposits incised on the Atacama Pediplain. The age constraints of volcanic ashes intercalated within Miocene sedimentary units range between 5.5 and 6.4 Ma (Fig. 4 & 5) (Mortimer et al., 1974; Naranjo & Paskoff, 1985; von Rotz et al., 2005; Kober et al., 2006; Hoke et al., 2007). We chose a maximum age of 7 Ma for the onset of incision that gives a minimum coastal incision rate, and thus a minimum uplift rate, of 0.14 mm/yr occurring over this period (see Fig. S1-B).

At the eastern side of the margin, the Western Cordillera is uplifting relatively to the Atacama Pediplain, due to the activity of west verging thrust fault systems that induce folding of a large ignimbritic cover of Miocene age and that also offsets underlying Jurassic and Cretaceous units (García et al., 2004; Pinto, 2004; Victor et al., 2004; Farías et al, 2005; Hoke et al., 2007; Jordan et al., 2010). Several local uplift rates relative to the CDB have been estimated for different periods of time. For example, an uplift rate of 0.02 mm/yr, accommodated by the West Vergent Thrust System, has been estimated for the last 8 My by [Farías et al., 2005]. The same authors estimated a higher uplift rate of 0.1 mm/yr for the same fault system but for the

period 11 to 8 Ma. [Jordan et al., 2010] estimated that 400 m of uplift has occurred since around 5 Ma across a wavelength monocline between 18°30'S and 22°S, that gives an uplift rate of 0.08 mm/yr. They also estimated an uplift of 810 m for the period 11 to 5 Ma, that gives an uplift rate of 0.13 mm/yr. So, to keep in agreement those different studies over the last 7 My, we chose a relative uplift rate of 0.08 mm/yr between the Western Cordillera and the Atacama Pediplain, to be consistent with the rate proposed by [Jordan et al., 2010] which concerns almost the same period of time. Therefore we set an absolute uplift rate of 0.22 mm/yr (= 0.14 + 0.08 mm/yr), for the eastern uplift rate over the last 7 My (see Fig. S1-B).

B.2 Initial topography

The Atacama Pediplain is an eroded and pediplanated shaped surface, over more than 500 km long, which had thus been a local or even a regional base level for the drainage system developed over the Western Cordillera going down from the Altiplano on the Atacama Pediplain (Figures 4 and 5 & S1-A). Fluvial deposits intercalated between ignimbrites of Miocene age (25 to 17 Ma) located close to the coast (Garcia, 2002) in the upper sedimentary units of the Atacama Bench indicate that a connection between the Atacama Bench to the ocean was probably established without being associated to deep incision (García, 2002). Moreover, the lack of marine sediments of Miocene or even younger age indicates that the surface was not below sea level. So, the Atacama Pediplain surface was probably located close to sea level before tectonic uplift (Kirk-Lawlor et al., 2013). The initial topography contains an initial flat coastal plateau located at sea level which is connected to the Altiplano plateau, with lower elevation at that time (eg. Hoke et al., 2007), by a constant western slope, in agreement with the simple shape derived with present-day topographic profiles (Fig. S1-C and S1-A).

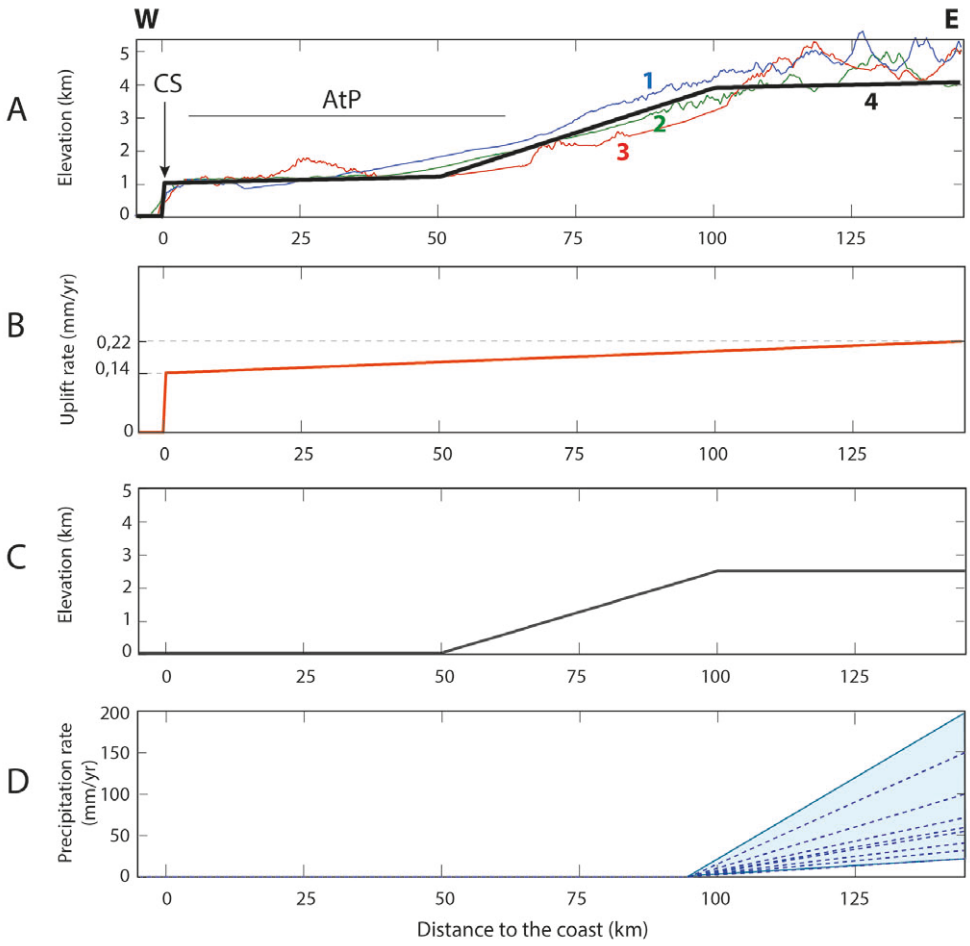

Fig. S1: Boundary conditions used in the numerical experiments.

A/ In color (1 to 3), topographic envelopes extracted from SRTM 3 data and corresponding to boxes 1 to 3 on Figure 6 of the paper; in black (4), simplified topographic profile. CS: Coastal Scarp; AtP: Atacama Pediplain.

B/ Uplift rate profile used for all the experiments. Near the CS, the rate is calculated from the average height of the CS (~1 km) divided by the age of the youngest incised sediments (≤7 Ma). For the eastern part of the profile, we consider a higher uplift rate to account for recent differential uplift of the Western Cordillera relatively to its piedmont (Victor et al., 2004; Farías et al., 2005; Hoke et al., 2007; Jordan et al., 2010). See text for detailed explanation.

C/ Initial topography set for all the experiments. The topographic profile is derived from the present-day topographic profile that is constrained over the threshold area, considering an uplift of 1 000 m of the margin over 7 My.

D/ Precipitation profiles tested in this study. All tested precipitation rates on the Western Cordillera (to the eastern side) stay in the overall range (20 to 200 mm/yr) than those that may be deduced from TRMM data over the threshold area (Fig. 6 of the paper; Bookhagen & Strecker, 2008).

C/ Model setting

C.1 Numerical experiments design

The parameters are summarized in Table S1. Explanation about the characterization of these parameters is given in section C.2

Parameters	Best fit model
Grid size (km^2)	200 * 150
Cell size (m^2)	500 * 500
Time step (yr)	10
Experiment duration (Myr)	7
Water flow routine	Multiple flow
Critical imposed water volume (m^3)	0
Water discharge (α) and slope (β) exponents	1,5 and 1
Alluvial transport K_{al} ($m^{-1,5}$ $y^{0,5}$)	2e-05
m and n exponents for the bedrock incision law	0,5 and 1
Diffusion coefficient for sediments κ_{sed} (m^2/yr)	5e-02
Diffusion coefficient for bedrock κ_{br} (m^2/yr)	5e-02
Critical slope parameter Sc_{sed} and Sc_{br}	tan(40°)and tan(80°)

Table S1: Model settings, boundary conditions and fixed parameters for our numerical experiments.

No water leaves the other two sides of the grid so water and sediments are evacuated towards the modeled ocean base level. Eroded sediments can either stay on the grid or be evacuated due to alluvial transport and diffusion as well as depositional processes on the sedimentary basin of the Atacama Bench in North Chile and transported by the Andean rivers.

C.2 Value constraint of the physical parameters

Parameters tested	Range of values		
Alluvial transport K_{al} ($m^{-1,5}$ $y^{-0,5}$)	$2\ 10^{-06}$	**$2\ 10^{-05}$**	$2\ 10^{-04}$
m and n exponents for the bedrock incision law	0,6 and 0,7	**0,5 and 1**	
Diffusion coefficient for sediments K_{sed} (m^2/yr)	$1\ 10^{-02}$	**$5\ 10^{-02}$**	$1\ 10^{-01}$
Diffusion coefficient for bedrock K_{br} (m^2/yr)	$1\ 10^{-02}$	**$5\ 10^{-02}$**	$1\ 10^{-01}$
Critical slope parameter $S_{c\ sed}$ and $S_{c\ br}$ (degrees)	30 and 60°	**40 and 80°**	

Table S2: Tested parameters. The selected values are outlined by grey boxes. The sensitivity to each parameter is tested independently by fixing the other parameters to their selected value, and for the K_{br} and Precipitation range used for our reference model. See Figures S2 to S4 and following explanation.

Water discharge exponent α are and slope exponent β values determine the degree of non-linearity of the transport law but they are not well constrained in the literature. Different values have nevertheless been reported and range between 0 and 2 (eg. Kooi & Beaumont, 1994; Allen & Densmore, 2000). Published analysis of the slope-area relationship suggests that the ratio $\frac{(\alpha-1)}{\beta}$ ranges between 0.3 and 0.7. We set the values of α and β equal to 1.5 and 1, respectively, as adopted by others studies using APERO for similar goal (Carretier & Lucazeau, 2005; Farías, 2007). In this case, the ratio $\frac{(\alpha-1)}{\beta}$ equals to 0.5.

Coefficient of the alluvial transport law K_{al} ($[L^{3-3\alpha}\, T^{\alpha-1}]$ ranges between $2e^{-06}$ to $2e^{-04}\, m^{-1,5}\, y^{0,5}$ as determined by previous theoretical studies (Tucker & Bras, 1998; Whipple et al., 2000; Tucker, 2004; Farías, 2008; Carretier et al., 2009). A small value of K_{al} ($2e^{-06}$) does not allow drainage incision to occur (Fig.S2). Inversely, a high value of K_{al} (2 orders of magnitude higher, $2e^{-04}$) enhances deposition of a large volume of sediments on the topography that prevents any river connection to the ocean (Fig.S2). We set K_{al} to $2e^{-05}\, m^{-1,5}\, y^{0,5}$ as an intermediate and pertinent value for river incision process in our model.

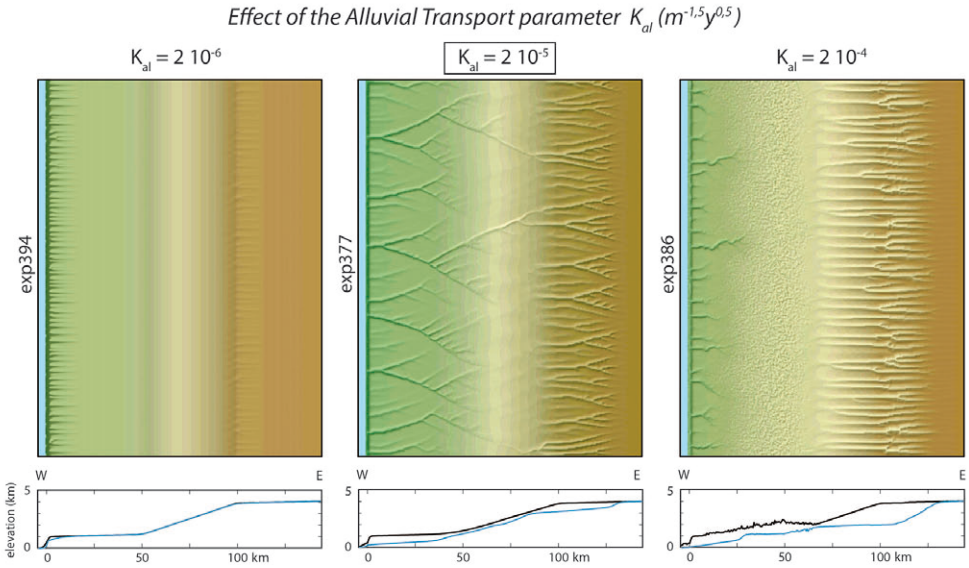

Fig. S2: Effect of the alluvial transport parameter. A small value of K_{al} [$m^{-1,5}$ $y^{0,5}$] (left) produces very limited incision, while a value higher by 2 orders of magnitude (right) induces aggradation of large volumes of sediments on top of the growing

coastal topography that prevents river connection to the ocean. We set K_{al} to a median value ($2e^{-05}\ m^{-1,5}\ y^{0,5}$, middle). On this figure and the following ones, the diagrams show modeled morphologies after 7 My. The maximum and minimum topographic envelopes, calculated over the entire grid, are shown in the graphs below. The selected value is boxed, and illustrated by the topography at the threshold for our reference model (Figure 8b of the paper, Figure S7 middle).

Water discharge exponent m and exponent of the slope n for the bedrock incision law are widely studied because they play a key role in river dynamics (Whipple & Tucker, 1999) and in the shape of the river knickpoint retreat (eg. Tucker & Whipple, 2002). Their values range between 0 and 2 and have to account for a $\frac{m}{n}$ ratio equal to 0.5 (eg. Stock & Montgomery, 1999). We set m equal to 0.5 and n equal to 1 (eg. Carretier, 2004) because these values account for the shape of parallel knickpoint retreat process as we observe in river profiles, North Chile (Carretier, 2004).

Erosion parameter of the bedrock incision law K_{br} is supposed to depend on lithologic resistance and erosion processes. It is not straightforward to set a value to K_{br} that fits well to natural conditions. This parameter is one of the more critical parameter in the drainage system development. In North Chile, we assume that lithology is constant longitudinally but varies from West to East, with Mesozoic sedimentary and volcanic sequences in the Coastal part, Oligo-Miocene volcano-sedimentary deposits in the Central part (AB) and a large Miocene volcanic sheet of ignimbrite covering the folded Mesozoic sedimentary and volcanic sequences observed also at the coast (Fig.7). Therefore, it is difficult to assess a unique value to K_{br} for the whole area. We tested a large range of values in the range of previous assumed values (eg. Stock & Montgomery, 1999; Van Der Beek & Bishop, 2003; Attal & Lavé, 2009; Carretier & Lucazeau, 2005; Farías, 2008). Our values of K_{br} range between $8e^{-07}$ and $5e^{-06}\ m^{-0,5}\ y^{-0,5}$. The influence of K_{br} is discussed in Section 4.1 and on Figures S5 to S9.

κ, the diffusive coefficient is often considered as a property of the altered material whose value changes with lithology, climate, and even grain size (Beaumont et al., 1992; Rivenaes, 1988). [Jordan and Flemings, 1989] differentiated between two diffusion coefficients for sediments and bedrock. This distinction also exists in APERO. Coefficient of diffusion for sediment κ_{sed} and for bedrock κ_{br} are both set here to $5e^{-02}\ m^2/yr$, compatible with the ranges of previous numerical studies and field estimates (between 10^{-04} to $10^{-01}\ m^2/yr$) (Hanks et al., 1984; Colman & Watson, 1984; Enzel et al., 1996; Martin, 2000). Furthermore, variations of κ_{sed} and of κ_{br} do not really have a major impact on the geometry of the drainage system nor on the river long profiles shape and incision depth as shown on Fig.S3 and Fig.S4, with all parameters taken constant.

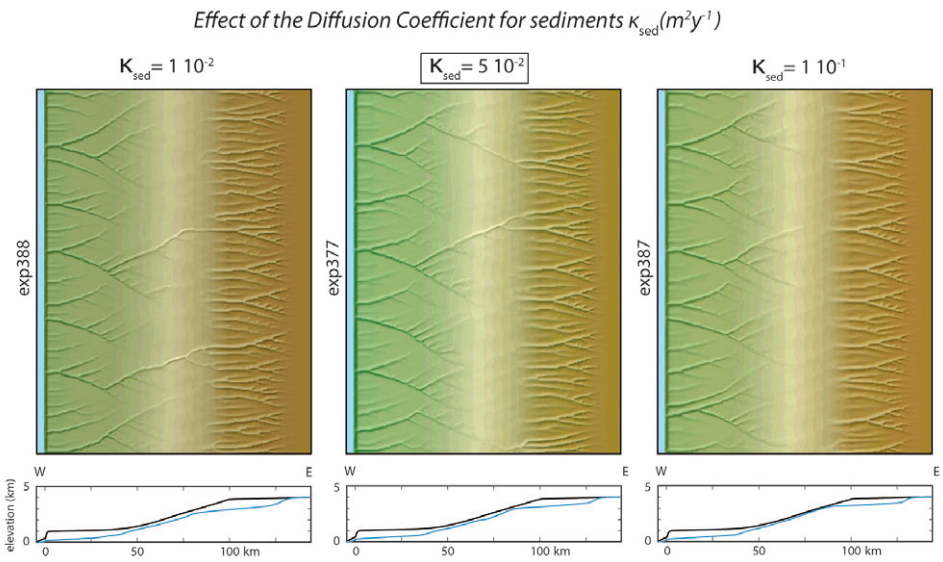

Fig. S3: Effect of the diffusion coefficient for sediments κ_{sed} $[m^2\ y^{-1}]$. Variations of this parameter have little effect, and the drainage geometry is roughly the same for the three tested values. We therefore use a median value.

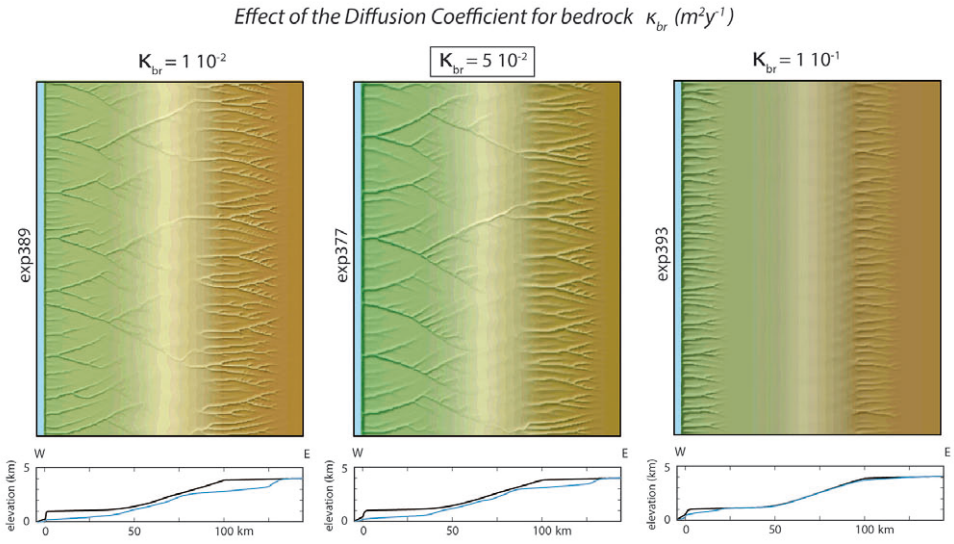

Fig. S4: Effect of the diffusion coefficient for bedrock κ_{br} $[m^2\ y^{-1}]$. The drainage geometry is roughly the same for the two lowest values (left and middle) while for the higher value (right), there is little incision and no links between the upper and lower river courses. We choose a median value for this parameter.

Critical gradient for sediments Sc_{sed} and for bedrock Sc_{br} are respectively set around 25° to 40° and around 60° to 75° in previous modeling studies for similar natural cases (eg. Tucker and Bras, 1998; Carretier, 2004; Farías, 2008; Pépin et al., 2010). We set Sc_{sed} to $(\tan 40°)$ and Sc_{br} to $(\tan 80°)$ to limit numerical effects as identified by [Carretier, 2004] and to preserve the steep shape of the Coastal Scarp and of the canyons flanks as we observe in North Chile.

D/ Sensitivity analysis

In the next descriptions, we show that our preferred solution (reference model) is not unique and that lithology and rainfall are intimately linked in the APERO numerical landscape model (Table S3). Nevertheless, considering a uniform lithology (ie. constant K_{br}), an increase in the precipitation rates influences river connection to the ocean whatever the erodibility value.

		Bedrock erosion coefficient K_{br} ($m^{-0,5}$ $y^{-0,5}$)		
		$8\ 10^{-07}$	$2\ 10^{-06}$	$5\ 10^{-06}$
Precipitation range (mm/yr)	20 - 40 - 60	NO	NO	YES *Fig. S9*
	30 - 55 - 70	NO *Fig. S6*	YES *Fig. S5*	NO *Fig. S7*
	70 - 100 - 150	YES *Fig. S8*	NO	NO

Table S3: Logical table resuming and illustrating the trade-off between erodibility (K_{br}) and Precipitation rates (PR). Indicated PR values are those occurring at the eastern border of the experimental box (see Fig.S1). Starting from our preferred, reference model (green white-boxed, Fig.S5) which uses median values, the experiments made with tougher and softer lithologies with similar PR range (Figures S6 and S7) give unsatisfactory results (in red on the Table S3). Yet, changing PR towards slightly higher (for tougher lithologies) or lower (for softer lithologies) ranges gives quite acceptable results given that experiments show that we can reproduce a geomorphic threshold such as the existing one in North Chile (in green on the table, Figures S8 and S9).

D.1 Influence of bedrock coefficient

Bedrock coefficient K_{br} represents rock erodibility and thus lithology. As it is difficult to assess an appropriate value for K_{br} to our natural case, the response of drainage development was tested for various values of K_{br}, listed in the literature, and for precipitation rates that range within the precipitation rates distribution of the threshold area: low (30 mm/yr), intermediate (55 mm/yr) and high (70 mm/yr) in the higher part of the topography (see profiles on Fig.S1).

For an intermediate lithology ($K_{br} = 2\mathrm{e}^{-06}\ \mathrm{m}^{-0,5}\ \mathrm{y}^{-0,5}$) (Fig.S5), an increase of the precipitation rates leads to a transition between endoreic and exoreic river systems across the topography (Fig.S5). Drainage system geometry is very similar to the North Chile river system with elongated and parallel rivers both for intermediate and higher precipitation rates. Projected longitudinal profiles at the transition state are concave up in the higher part of the

topography, then are very close to the topographic slope, showing a knickpoint at the junction between the base of the topographic slope and the eastern limit of the coastal plateau and finally become concave up towards the ocean base level. This behavior is comparable to the Tiliviche river profile. For higher precipitation rates, river canyons are deeply entrenched into the topography showing a concave up river profile similar to the northern exoreic rivers in North Chile.

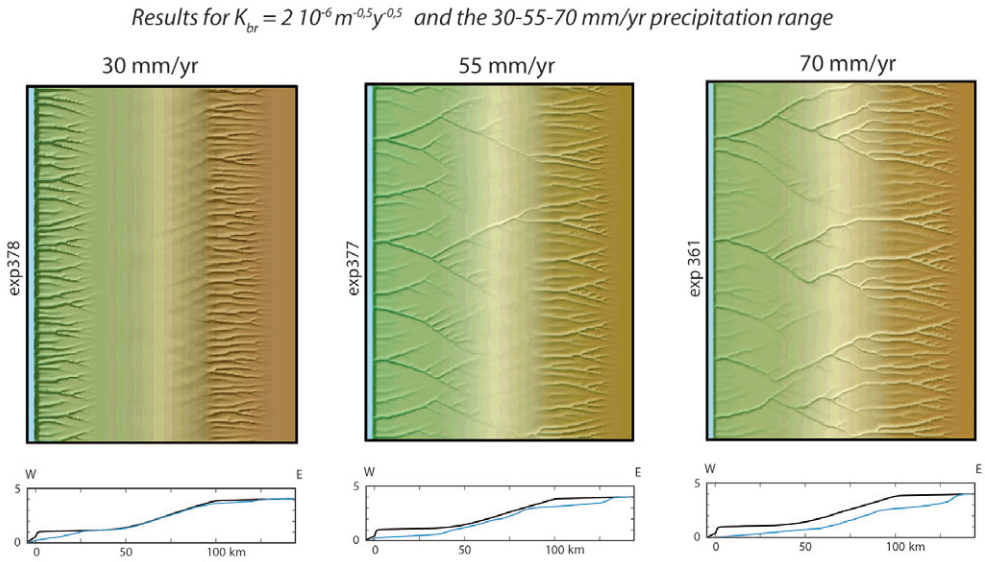

Fig.S5: Selected reference model (Fig.8b of the paper) with ($K_{br} = 2\mathrm{e}^{-06}\ \mathrm{m}^{-0,5}\ \mathrm{y}^{-0,5}$) and PR is the 30-55-70 mm/yr range. Left, middle and right diagrams fit well the natural morphologies south of, at, and north of the natural threshold, respectively (see Fig.8b of the paper).

For a "tougher" lithology ($K_{br} = 8\mathrm{e}^{-07}\ \mathrm{m}^{-0,5}\ \mathrm{y}^{-0,5}$), with all parameters taken constant, there is no connection between higher and coastal drainage systems for the range of precipitation rates we used (Fig.S6).

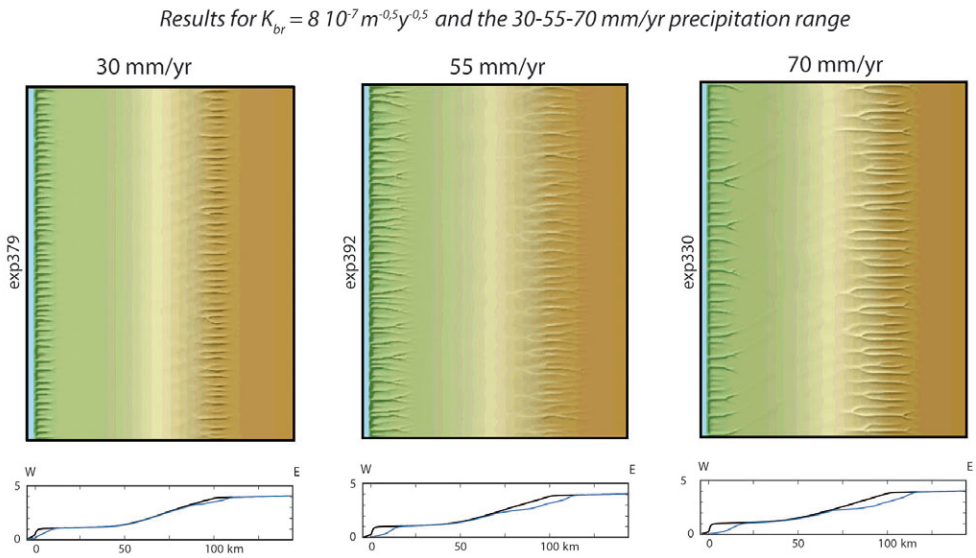

Fig.S6: Experiments with tougher lithology ($K_{br} = 8e^{-07}\ m^{-0,5}\ y^{-0,5}$) and same PR than for the reference model. These experiments are unable to reproduce the natural threshold as there is no link between the upper and lower river courses in any case.

For a "softer" lithology, ($K_{br} = 5e^{-06}\ m^{-0,5}\ y^{-0,5}$), drainage system is endoreic for lower precipitation rates but is highly developed at the coast and on the coastal plateau (Fig.S7). For intermediate precipitation rates, the system is totally exoreic and presents a similar geometry to the north Chile river system (see Fig.2). River profiles do not present the knickpoint we observed at the base of the topographic slope in the previous case. For higher precipitation rates, drainage geometry did not change but the higher part of the topography is dramatically incised over more than 1 km depth.

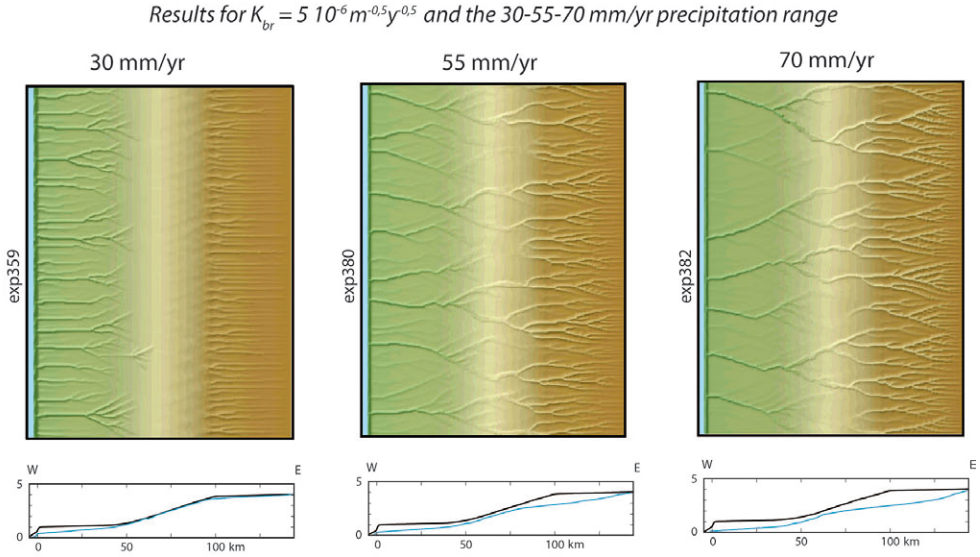

Fig.S7: Experiments with softer lithology ($K_{br} = 5e^{-06}\ m^{-0,5}\ y^{-0,5}$) and same PR than for the reference model. These experiments hardly reproduce the natural

threshold because we observe a systematic tight connection between the upper and lower river courses, for both the 55 and 70 mm/yr PR (middle and right).

Compared to the north Chile river system geometry and river canyons shapes described in the main paper (Fig.2), the intermediate bedrock coefficient ($K_{br} = 2e^{-06}\ m^{-0,5}\ y^{-0,5}$) is the best appropriated value to represent the north Chile threshold area lithology. We consider this model as our reference model with the following precipitation rates: 30, 55 and 70 mm/yr in the higher part of the topography (Fig.S5).

D.2 Erodibility and precipitation rates trade-off

We have shown in the previous section that for a "tough" lithology ($K_{br} = 8e^{-07}\ m^{-0,5}\ y^{-0,5}$), any river system is well developed across the topography. In fact, there is a trade-off between precipitations and erodibility, as indicated by the stream power equation for bedrock incision (Eq.SI4). With the same value of K_{br} , and for higher precipitation rates, the river system developed over the modeled area can change from endoreic to exoreic (Fig.S8). The geometry of the drainage is quite similar to our reference model although river incision does not propagate further into the higher plateau. Projected river profiles are similar to the projected river profiles of the reference model except for higher precipitation rates where river profile is not concave up all along the profile (Fig.S8). Furthermore, incision is exaggerated relatively to North Chile river profiles.

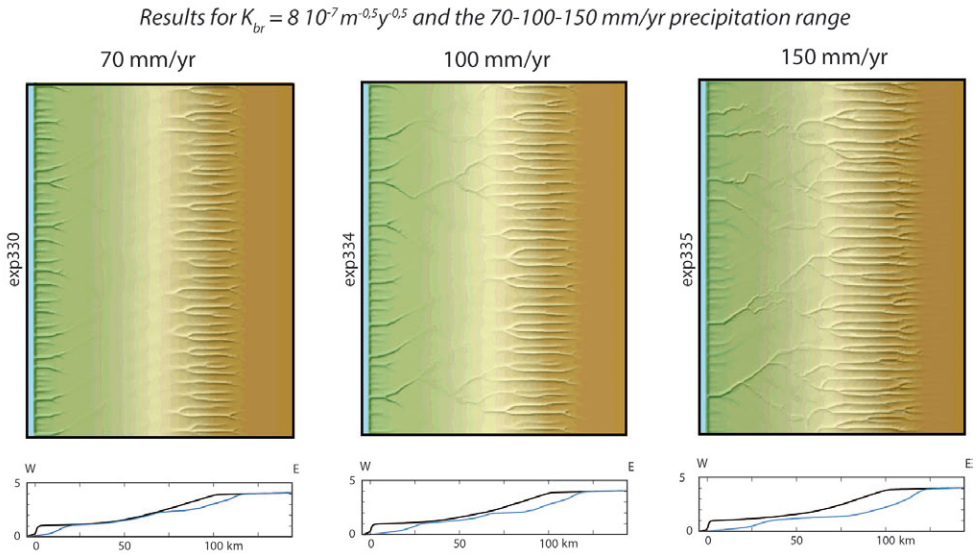

Fig.S8: Experiments with tougher lithology ($K_{br} = 8e^{-07}\ m^{-0,5}\ y^{-0,5}$) and higher PR than for the reference model. These experiments are able to produce the geomorphic threshold.

For a "smooth" lithology, the precipitation rates we used in the previous part were too high to observe and constrain the threshold of river connection to the ocean. Therefore, precipitation range that allows us to observe the transition should be lower than the one used in the reference

model. We tested smaller values (20, 40 and 60 mm/yr in the higher topographic part). The results are shown on Fig.S9. The connection threshold is well illustrated in these experiments where erodibility is low.

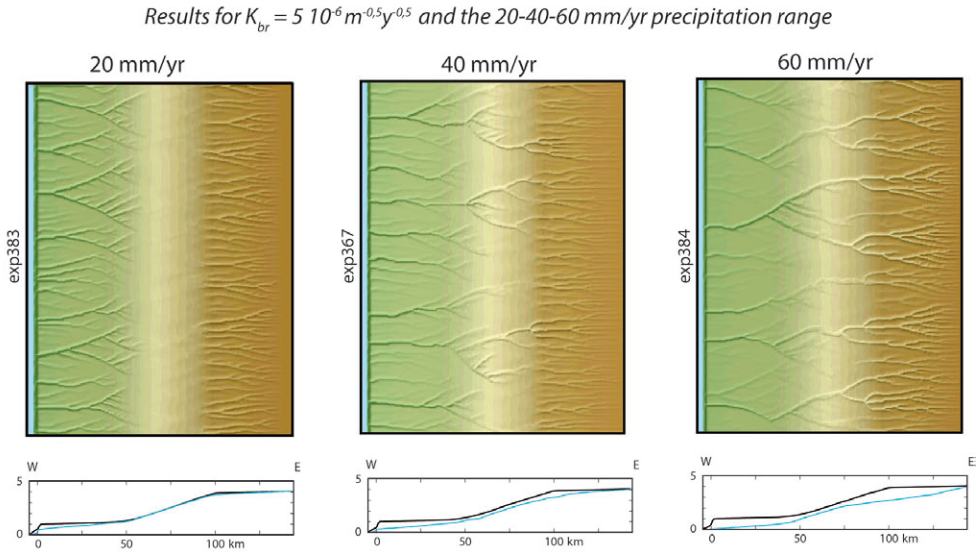

Fig.S9: Experiments with softer lithology ($K_{br} = 5e^{-06}\ m^{-0,5}\ y^{-0,5}$), and lower PR than for the reference model. These experiments better reproduce the natural threshold than those shown on Fig.S7, but with more dendritic and branching river systems than for the reference model.

E/ Influence of the initial coastal topography

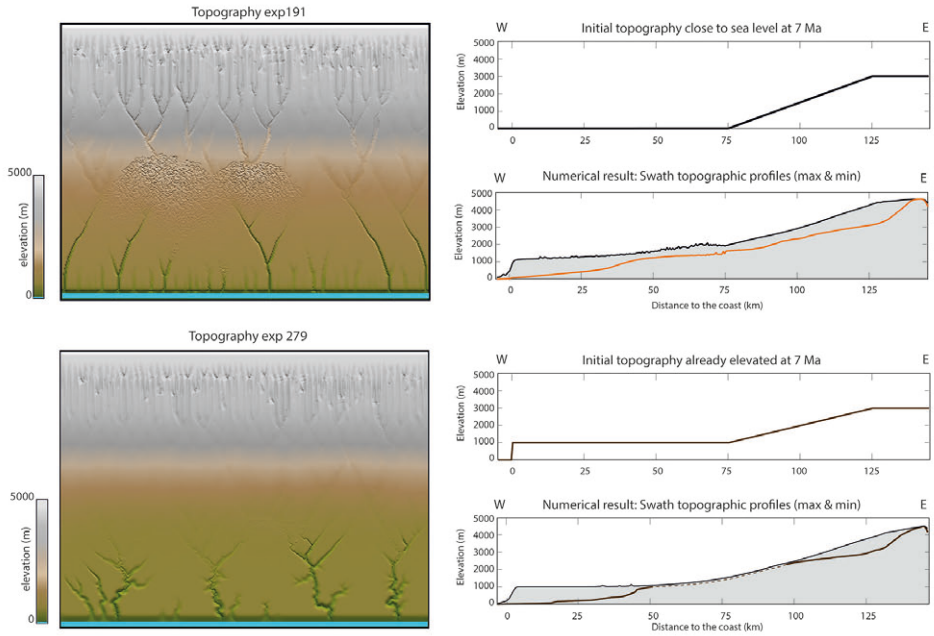

Fig.S10: Influence of the initial topography, close to sea level (top) vs. already elevated at 7 Ma (bottom), on river drainage development. Precipitation Rates : 140 mm/yr on the higher plateau. The same constant uplift rate has been applied to

both topographies, except on the lower plateau for the elevated initial topography. All parameters are taken constant between the two experiments. Note the clear difference of the shape of the river network developed onto the coastal plateau: elongated and narrow drainage network vs. meandering and spread drainage network. It seems that tectonic uplift is a major driver for the formation of straight elongated channels, as we observe in North Chile.

F/ References cited in Supplementary Information

Allen, P.A., and Densmore, A.L., 2000, Sediment flux from an uplifting fault block, Basin Research, v. 12, p. 367-380.

Attal, M., and Lavé, J., 2009, Pebble abrasion during fluvial transport: Experimental results and implications for the evolution of the sediment load along rivers: Journal of Geophysical Research, v. 114, F04023, doi: 10.1029/2009JF001328.

Beaumont, C., Fullsack, P. and Hamilton, J., 1992, Erosional control of active compressional orogens, in McClay, K.R., ed., Thrust tectonics: New York, Chapman and Hall, p.1-18

Braun, J. and Sambridge, M., 1997, Modelling landscape evolution on geological time scales: a new method based on irregular spatial discretization, Basin Research, 9: 27-52

Bookhagen, B., and Strecker, M.R., 2008, Orographic barriers, high‐resolution TRMM rainfall, and relief variations along the eastern Andes: Geophysical Research Letters, v. 35, no. 6, L06403, doi: 10.1029/2007GL032011.

Carretier, S., 2000, Cycle sismique et surrection de la chaîne de Gurvan Bogd (Mongolie). Approche de la géomorphologie quantitative, Ph.D. thesis, Université Montpellier 2

Carretier, S., 2004, Apero user's guide: Hazard Mechanisms and Simulation Unit, Development Planning and Natural Risks Division, BRGM Orléans.

Carretier, S. and Lucazeau, F. 2005, How does alluvial sedimentation at range fronts modify the erosional dynamics of mountain catchments?: Basin Research, v. 17, p. 361–381, doi: 10.1111/j.1365-2117.2005.00270.x

Carretier, S., Poisson, B., Vassallo, R., Pépin, E., Farías, M., et al., 2009, Tectonic interpretation of transient stage erosion rates at different spatial scales in an uplifting block: J. Geophys. Res, v. 114, F02003, doi: 10.1029/2008JF001080.

Colman, S.M., and Watson, K., 1984, Ages estimated from a diffusion equation model for scarp degradation, Science, v.221, p. 263-265

Coulthard, T.J., Macklin, M.G. and Kirkby, M.J., 2002, A cellular model of Holocene upland river basin and alluvial fan evolution, Earth Surface Processes and Landforms, v.27, n.3, p, 269-288

Crave, A., and Davy, P., 2001, A stochastic « precipiton » model for simulating erosion/sedimentation dynamics, Computers & Geosciences, v. 28, p. 815-827

Davy, P., and Crave, A., 2000, Upscaling local-scale transport processes in large-scale relief dynamics, Physics and Chemistry of the Earth, Part A: Solid Earth and Geodesy, 25(6–7), 533-541, doi:10.1016/S1464-1895(00)00082-X.

Enzel, Y., Amit, R., Porat, N., Zilberman, E., and Harrison, B.J., 1995, Estimating the ages of fault scarps in the Arava, Israel, Tectonophysics, v. 253, p. 305-317

Farías, M., 2007, Tectonique, érosion et évolution du relief dans les Andes du Chili Central au cours du Néogene, Ph.D. thesis, Université Paul Sabatier, Toulouse

Farías, M., Charrier, R., Comte, D., Martinod, J., and Hérail, G., 2005, Late Cenozoic deformation and uplift of the western flank of the Altiplano: Evidence from the depositional, tectonic, and geomorphologic evolution and shallow seismic activity (northern Chile at 19°30'S): Tectonics, v. 24, TC4001, doi: 10.1029/2004TC001667.

Farías, M., Charrier, R., Carretier, S., Martinod, J., Campbell, D., Cáceres, J., and Comte, D., 2008, Late Miocene high and rapid surface uplift and its erosional response in the Andes of Central Chile (33°-35°S): Tectonics, v. 27, TC1005, doi: 10.1029/2006TC002046

García, M., 2002, Evolution Oligo-Miocène de l'altiplano occidental (Arc et Avant-arc du Nord Chili, Arica): Tectonique, volcanisme, sédimentation, géomorphologie et bilan érosion-sédimentation, Ph.D. thesis, Laboratoire de géodynamique des Chaînes alpines de l'Université Joseph Fourier de Grenoble

García, M., Gardeweg, M., Clavero, J., Hérail, G., and S. N. de Geología y Minería, 2004, Hoja Arica, Region de Tarapacá, Carta Geologica de Chile, 84

Hanks, T. C., Buckham, R. C., LaJoie, K. R., Wallace,R. E., 1984, Modification of wave-cut and fault-controlled landforms, Journal of Geophysical Research, v.89, p.5771–5790

Hoke, G.D., Isacks, B.L., Jordan, T.E., Blanco, N., Tomlinson, A.J., and Ramezani, J., 2007, Geomorphic evidence for post-10 Ma uplift of the western flank of the central Andes 18°30′-22°S, Tectonics, v. 26, p. 17, doi: 10.1029/2006TC002082.

Jordan, T.E., and Flemings, P.B., 1989, From geodynamic models to basin fill - a stratigraphic perspective, in Quantitative Dynamic Stratigraphy, edited by T. Cross, Prentice Hall, Englewood Cliffs, New Jersey.

Jordan, T. E., P. L. Nester, N. Blanco, G. D. Hoke, F. Dávila, and A. J. Tomlinson, 2010, Uplift of the Altiplano-Puna plateau: A view from the west, Tectonics, 29, TC5007, doi: 10.1029/2010TC002661.

Kirk-Lawlor, N. Jordan, T.E., Rech, J.A., and Lehmann, S., 2013, Late Miocene to Early Pliocene paleohydrology and landscape evolution of Northern Chile, 19° to 20°S, Palaeogeography, Palaeo-climatology, Palaeoecology, 387: 76-90

Kober, F., Schlunegger, F., Zeilinger, G., and Scheider, H., 2006, Surface uplift and climate change : The geomorphic evolution of the Western Escarpment of the Andes of northern Chile between the Miocene and present: GSA Special Papers 2006, v. 398, p.75-86, doi: 10.1130/2006.2398(05).

Kooi, H. and Beaumont, C., 1994, Escarpment evolution on a high-elevation rifted margins: insights derived from a surface processes model that combines diffusion, advection, and reaction, Journal of Geophysical Research, v. 99 (B6), p. 12191-12209

Martin, Y., 2000, Modelling hillslope evolution: linear and nonlinear transport relations, Geomorphology, v. 34, p.1-21

Mortimer, C., Farrar, E., and Saric, N., 1974, K-Ar ages from Tertiary lavas of the northernmost Chilean Andes, Geologische Rundschau, v. 63(2), p.484-490

Naranjo, J.A., and Paskoff, R., 1985, Evolución cenozoica del piedemonte andino en la Pampa del Tamarugal, norte de Chile (18°-21°S): In IV Congreso Geologico Chileno, volume 4, pages 5–149 – 5–165. Universidad del Norte de Chile.

Pépin, E., Carretier, S., and Hérail, G., 2010, Erosion dynamics modelling in a coupled catchment-fan system with constant external forcing: Geomorphology, v. 122, p. 78–90, doi: 10.1016/j.geomorph.2010.04.029.

Pinto, L., 2004, Sedimentacion sintectonica asociada a las estructuras neogenas en la Precordillera de la zona de Moquella, Tarapaca (19°15'S, norte de Chile), Revista geologica de Chile, v. 31(1), p.19-44

Quezada, J., 2008, Interacción entre procesos tectónicos y procesos erosivos en la configuración del relieve litoral del Norte de Chile, Ph.D. thesis, Universidad Católica del Norte, Chile

Rivenaes, J.C., 1988, Application of a dual-lithology, depth dependent diffusion equation in stratigraphic simulation, Basin Research, v.4, p. 133-146

Roering, J.J., Kirchner, J.W., and Dietrich, W.E., 1999, Evidence for non-linear, diffusive sediment transport on hillsplopes and implications for landscape morphology, Water Resources Research, v.35, p.853-870

Stock, J.D., and Montgomery, D.R., 1999, Geologic constraints on bedrock river incision using the stream power law: Journal of Geophysical Research, v. 104, p. 4983–4993, doi: 10.1029/98JB02139.

Tucker, G.E., and Whipple, K.X., 2002, Topographic outcomes predicted by stream erosion models: Sensitivity analysis and intermodel comparison: Journal of Geophysical Research, v. 107, 2179, doi: 10.1029/2001JB000162.

Tucker, G. E., 2004, Drainage basin sensitivity to tectonic and climatic forcing: implications of a stochastic model for the role of entrainment and erosion thresholds: Earth Surface Processes and Landforms, v. 29, p. 185–205, doi: 10.1002/esp.1020.

Tucker, G. E., and Bras, R. L., 1998, Hillslope processes, drainage density, and landscape morphology: Water Resources Research, v. 24, p. 2751–2764, doi: 10.1029/98WR01474.

Tucker, G.E., and Bras, R.L., 2000, A stochastic approach to modeling the role of rainfall variability in drainage basin evolution, Water Resources Research, 36(7): 1953-1964

Tucker, G.E., and Slingerland, R.L., 1994, Erosional dynamics, flexural isostasy, and long-lived escarpments: a numerical modeling study, Journal of Geophysical Research, 99: 12 229-12 243

Tucker, G.E., and Whipple, K.X., 2002, Topographic outcomes predicted by stream erosion models: Sensitivity analysis and intermodel comparison, Journal of Geophysical Research, v.107, B9, doi: 10.1029/2001JB000162

Van De Wiel, M.J., Coulthard, T.J., Macklin, M.G. and Lewin, J., 2007, Embedding reach-scale fluvial dynamics within the CAESAR cellular automaton landscape evolution model, Geomorphology, 90: 283-301

Van der Beek, P., and Braun, J., 1999, Controls on post-mid-Cretaceous landscape evolution in the southeastern highlands of Australia: Insights from numerical surface process models,

Journal of Geophysical Research, v. 104, 4945-4966

Van der Beek, P., and Bishop, P., 2003, Cenozoic river profile development in the Upper Lachlan catchment (SE Australia) as a test of quantitative fluvial incision models: Journal of Geophysical Research, v. 108, 2309, doi: 10.1029/2002JB002125.

Victor, P., Oncken, O., and Glodny, J., 2004, Uplift of the western Altiplano plateau: Evidence from the Precordillera between 20 and 21 S (northern Chile): Tectonics, v. 23, p. Tc4004, doi: 10.1029/2003TC001519.

Von Rotz, R., Schlunegger, F., Heller, F., and Villa, I., 2005, Assessing the age of relief growth in the Andes of northern Chile: Magneto-polarity chronologies from Neogene continental sections: Terra Nova, v. 17, p. 462–471, doi: 10.1111/j.1365-3121.2005.00634.x.

Whipple, K. X., and Tucker, G. E., 1999, Dynamics of the stream-power river incision model: Implications for height limits of mountain ranges, landscape response timescales, and research needs: Journal of Geophysical Research, v. 104, p. 17661-17674, doi: 10.1029/1999JB900120.

Whipple, Kelin X., Hancock, Gregory S., Anderson, Robert S., 2000a, River incision into bedrock: Mechanics and relative efficacy of plucking, abrasion and cavitation, Geological Society of America Bulletin, v. 112, n. 3, p. 490-503.

Willgoose, G.R., Bras, R.L., Rodriguez-Iturbe, I., 1991a, A physically based coupled network growth and hillslope evolution model: 1 Theory, Water Resources Research, 27(7):1671-1684